J Mater Sci (2012) 47:7978–7985
DOI 10.1007/s10853-012-6687-5

Room temperature elastic moduli and Vickers hardness of hot-pressed LLZO cubic garnet

Jennifer E. Ni · Eldon D. Case · Jeffrey S. Sakamoto · Ezhiyl Rangasamy · Jeffrey B. Wolfenstine

Received: 16 March 2012 / Accepted: 19 June 2012 / Published online: 6 July 2012

Abstract Cubic garnet $Li_{6.24}La_3Zr_2Al_{0.24}O_{11.98}$ (LLZO) is a candidate material for use as an electrolyte in Li–Air and Li–S batteries. The use of LLZO in practical devices will require LLZO to have good mechanical integrity in terms of scratch resistance (hardness) and an adequate stiffness (elastic modulus). In this paper, the powders were fabricated by powder processing of cast ingots. All specimens were then densified via hot pressing. The room temperature elastic moduli (Young's modulus, shear modulus, bulk modulus, and Poisson's ratio) and hardness were measured by resonant ultrasound spectroscopy, and Vickers indentation, respectively. For volume fraction porosity, P, the Young's modulus was 149.8 ± 0.4 GPa ($P = 0.03$) and 132.6 ± 0.2 GPa ($P = 0.06$). The mean Vickers hardness was 6.3 ± 0.3 GPa for $P = 0.03$ and 5.2 ± 0.4 for $P = 0.06$.

Introduction

Recently, there has been interest in the development of Li–Air and Li–S batteries for high energy applications [1]. One Li–Air configuration involves the use of a lithium anode in a non-aqueous electrolyte, which is separated from an aqueous electrolyte containing the air cathode by a solid state Li-ion conducting membrane [2–4]. For the case of Li–S, a possible configuration involves a solid Li-ion-conducting membrane separating molten lithium from molten sulfur.

To be used as a membrane in these situations, the material must have high relative density, high total Li-ion conductivity, and good chemical stability. In addition, the material should also exhibit good mechanical properties. The elastic moduli are needed for stress–strain calculations, and hardness is a measure of the resistance to scratching and point contact damage. For example, both Young's modulus and Poisson's ratio are often used to construct stiffness matrices for stress–strain calculations via finite element analyses [5]. Cubic $Li_7La_3Zr_2O_{12}$ (LLZO) has recently become of interest as a possible membrane material for Li–Air and Li–S batteries. There have been studies on the ionic conductivity and chemical stability of cubic $Li_7La_3Zr_2O_{12}$ prepared by powder processed and chemical methods (i.e., Pechini) [6–10].

No mechanical properties are available in the literature for cubic LLZO garnet materials. This study is the first to report the Young's modulus, shear modulus, bulk modulus, and hardness of dense, hot-pressed cubic $Li_{6.24}La_3Zr_2Al_{0.24}O_{11.98}$.

Experimental procedure

Specimen preparation

Lithium carbonate (Puratronic 99.998 %, Alfa Aesar), lanthanum(III) hydroxide (99.95 %, Alfa Aesar), zirconium oxide (99.9 %, Inframat Advanced Materials LLC), and gamma aluminum oxide (99.9 %, 50 nm, Mager Scientific Inc.) precursors were used to synthesize single-phase cubic $Li_{6.24}La_3Zr_2Al_{0.24}O_{11.98}$ (LLZO) [11]. The precursors were mixed in an agate milling vial using a

J. E. Ni · E. D. Case (✉) · J. S. Sakamoto · E. Rangasamy
Chemical Engineering and Materials Science Department, Michigan State University, Room 2527 Engineering Building, East Lansing, MI 48824-1226, USA
e-mail: casee@egr.msu.edu

J. B. Wolfenstine
Army Research Laboratory, RDRL-SED-C, 2800 Powder Mill Road, Adelphi, MD 20783, USA

Retsch PM-100 planetary mill. After mixing, the powders were loaded into a stainless steel die and cold pressed into pellets at 100 MPa. The pellets were placed in boron nitride-coated Al_2O_3 combustion boats (Coors Combustion boat from Sigma Aldrich), fired in air at 1000 °C for 4 h, and reground in an agate milling vial using a Retsch PM-100 planetary mill. The boron nitride coating prevented the reaction between the Al_2O_3 crucible and the LLZO pellets. The reground LLZO powders were hot pressed at 1000 °C under 40 MPa pressure for 1 h under flowing argon. The resulting pellet was removed from the hot press and heated in air at 1000 °C for 4 h to burn off residual graphite from the hot pressing die. The LLZO specimens were mounted in Crystalbond wax (Buehler, Lake Bluff, Il) and cut into rectangular parallelepipeds using a diamond saw.

The bulk densities of the rectangular parallelepiped hot-pressed specimens were determined from the mass and dimensions (Table 1) measured using a micrometer (Mitutoyo, 293-832, Aurora, IL) and an electronic balance (Ohaus Adventurer, AR2140, Pinebrook, NJ). The electronic balance and the micrometer were calibrated using commercial test weights (1, 2, 5 and 10 g, Tromner ASTM class 7) and gauge blocks (ranging in dimension from 1 to 20 mm, Mitutoyo Grade 0), respectively.

The relative density values, and hence the porosity was determined by dividing the bulk density by the ρ_{theo} of cubic Al-containing LLZO ($\sim$5.107 g/cm^3 [9]). Four crescent-shaped specimens were cut from the edges of the disk-shaped hot-pressed billets. The resulting parallelepiped specimens were used for elasticity measurements and the crescent-shaped specimens were used for hardness testing (Table 1). Each of the hardness and elasticity specimens were polished using successively smaller diamond paste with grit sizes down to one micron (Diamond polishing compounds, Leco, St. Joseph, MI).

X-ray diffraction and scanning electron microscopy (SEM)

The microstructure of the hot-pressed specimens was examined on uncoated fracture surfaces by SEM with an accelerating voltage of 1 and 3 kV. Phase purity was evaluated from X-ray diffraction data obtained using a Rigaku Ultima III diffractometer with Cu K_α radiation. The lattice constant was determined by obtaining the diffraction data in parallel beam geometry and fitting the data by Rietveld refinement [12] by means of RIQAS software (Materials Data Inc.).

Vickers indentation measurements

The Vickers hardness, H, was measured using a Shimadzu hardness tester (Shimadzu HMV-2000, Kyoto, Japan). Before indentation, the indenter was calibrated using a commercially available standard hardness block (761-048, Yamamoto Scientific Tools Lab, Co., Ltd, Japan). The average hardness of the LLZO specimens was determined using ten indentations per load on the polished surface at loads of 2.9 and 4.9 N with a 5 s loading time. To avoid the interference between stress fields of closely spaced indentations or perturbations caused by specimen edge effects, separation distances of at least 500 μm were maintained between adjacent indentation sites. No indentations were placed closer than roughly 1000 μm from the nearest free edge of the specimen. The H values were calculated by

$$H = \frac{1.8544F}{(2a)^2} \quad (1)$$

where F is the applied force and $2a$ is the diagonal of the diamond indentation impression [13].

Table 1 The specimen geometry, dimensions, mass, density, volume fraction porosity, P, and measurement techniques for the LLZO rectangular parallelepiped, RP, and crescent-shaped, CR, specimens included in this study

Specimen label	Specimen geometry	Dimensions (mm)	Mass (g)	Density (g/cm^3)	P	Measurement technique
LLZO-01a	RP	7.9 × 6.3 × 2.8	0.704	4.97	0.03	RUS
LLZO-01b	CR	9.0 × 4.5[a]	NA[b]	NA[b]	NA[b]	Vickers indentations
LLZO-02a	RP	8.0 × 7.1 × 2.5	0.687	4.78	0.06	RUS
LLZO-02b	CR	7.3 × 2.7[a]	NA[b]	NA[b]	NA[b]	Vickers indentations
LLZO-02c	CR	8.2 × 3.0 [a]	NA[b]	NA[b]	NA[b]	Vickers indentations

The specimens were powder processed from ingot and densified by hot pressing. The elastic moduli were measured by resonant ultrasound spectroscopy (RUS) and the hardness was measured via Vickers indentations

[a] Dimensions refer to length and maximum width of the crescent-shaped specimens

[b] Not available

Resonant ultrasound spectroscopy (RUS) measurements

RUS has been used to determine the elastic moduli for numerous ceramics and metals [14–32]. In particular, the Quasar hardware used in this study (RUSpec, Magnaflux Quasar, Albuquerque, NM) has been used to measure the elastic moduli of a variety of solid materials including the thermoelectric materials PbTe–PbS [15], PbTe [16, 17, 19], oxides such as alumina [14], hydroxyapatite [14], langatates [20], $La_{0.5}Sr_{0.5}Fe_{1-x}Co_xO_{3-\delta}$ perovskites [22], $SmScO_3$ [23], and $NdScO_3$ [23], a number of ternary and quaternary carbides such as Ti_3SiC_2 [27], Ti_3GeC_2 [27], $Ti_3Si_{0.5}Al_{0.5}C_2$ [27], Ti_2AlC [27], and Ti_3SiC_2 [31], metallic materials including single crystal fcc Al [25] and 4140-steel [29] as well as composites such as Al/Al_2O_3 [30] and Ni–YSZ cermets [27]. The RUS apparatus used in this study consists of a computer (Magnaflux Quasar, Albuquerque, NM) that controls the transceiver (Magnaflux Quasar RI 2600 Transceiver, Magnaflux Quasar, Albuquerque, NM) by means of commercial software (Galaxy, Magnaflux Quasar, Albuquerque, NM). The RUS system includes three lead zirconate titanate ceramic transducers. The transceiver drives one transducer and then collects the specimen's mechanical vibrations through the other two transducers. The RUS specimen is simply supported by the tripod of transducers and contracts the transducers via a SiC wear tip that is bonded to each transducer.

Results and discussion

Microstructure and lattice parameter of LLZO specimens

In this study, the LLZO microstructure was observed on a (i) fracture surface of LLZO-01 (Fig. 1a) and (ii) at five sites approximately three mm apart along a diametral fracture for LLZO-02 (Fig. 1b–e). The fracture surfaces of hot-pressed LLZO-01 and 02 had equiaxed grains with average grain sizes of 4.5 and 5.0 μ, respectively (Fig. 1a, c–e), which was measured by the linear intercept method with a stereographic projection factor of 1.5 [33]. The pores were spherical or quasi-spherical with diameters ranging from submicron to roughly 3 μ. Thus, the microstructure appeared to be homogenous for the two hot-pressed LLZO specimens included in this study (Fig. 1).

X-ray diffraction confirmed that after hot-pressing the pellet was single-phase cubic LLZO. After burning off the graphite residue, the pellet appeared bright white. Applying Rietveld analysis to the X-ray-diffraction data yielded a lattice parameter value, a_0, of 12.9773 Å for the single-phase cubic $Li_{6.24}La_3Zr_2Al_{0.24}O_{11.98}$ included in this study.

Elastic moduli measured via RUS

With RUS, the mechanical vibrational spectra of two hot-pressed LLZO specimens were measured (Tables 1, 2) over the frequency interval from 150 to 1000 kHz. The elastic moduli were calculated by means of commercially available software. The two hot-pressed LLZO specimens were assumed to be isotropic in part since the anisotropy induced by hot pressing of the planetary-milled powders is usually small. In addition, fracture sections of LLZO-01 (Fig. 1a) and LLZO-02 (Fig. 1b–d) are equiaxed, showing no observable anisotropic deformation induced by the hot press. In addition, a polished cross section of a LLZO-01 shows quasi-spherical porosity (Fig. 2), again with no indication of morphological texturing induced by hot pressing.

In terms of possible perturbations on the modulus measurements due to contact forces, the mass of each of the RUS specimens was approximately 0.7 g (Table 1). Since each specimen was simply supported on a transducer tripod, this means a loading of about 0.23 g on each transducer or a gravitational force of approximately 2.3×10^{-3} N per transducer. We assume that contact forces on the order of a few mN per transducer are not a significant source of perturbation.

In addition, from the literature, a comparison can be made between the elastic moduli obtained from polycrystalline PbTe measured by RUS [16] (on PbTe specimens of comparable mass to those LLZO specimens used in this study) and the aggregate average modulus (mean of the Hashin–Shtrikman bounds [16]) calculated from single crystal PbTe measured by ultrasonic pulse echo [34–36]. At approximately 300 K, the elastic moduli agreed to within 2–3 % when measured by RUS [16] or calculated from the aggregate average of the single crystal data for the ultrasonic pulse echo measurements [34–36]. Therefore, for the RUS PbTe measurements [16], the total effective error due to contact forces, specimen machining, cracks, or equipment artifacts and other sources should be on the order of roughly 2–3 %. Since this study employs the same hardware and software as was used in the RUS study of PbTe [16], we assume that roughly the same error bound applies to RUS measurements in this study.

Table 2 compares the data for elastic moduli for LLZO from this study to polycrystalline yttrium iron garnets from the literature [37, 38].

In this study, for the specimen with $P = 0.03$, the Young's modulus, E, shear modulus, G, bulk modulus, B, and Poisson's ratio, ν, were 149.8 ± 0.4, 59.6 ± 0.1, 102.8 ± 0.3 GPa and 0.257, respectively (Table 2). For $P = 0.06$, $E = 132.6 \pm 0.2$ GPa, $G = 52.1 \pm 0.04$ GPa, $B = 97.7 \pm 0.2$ GPa, and $\nu = 0.274$, respectively (Table 2). The elastic moduli decreased with increasing porosity in

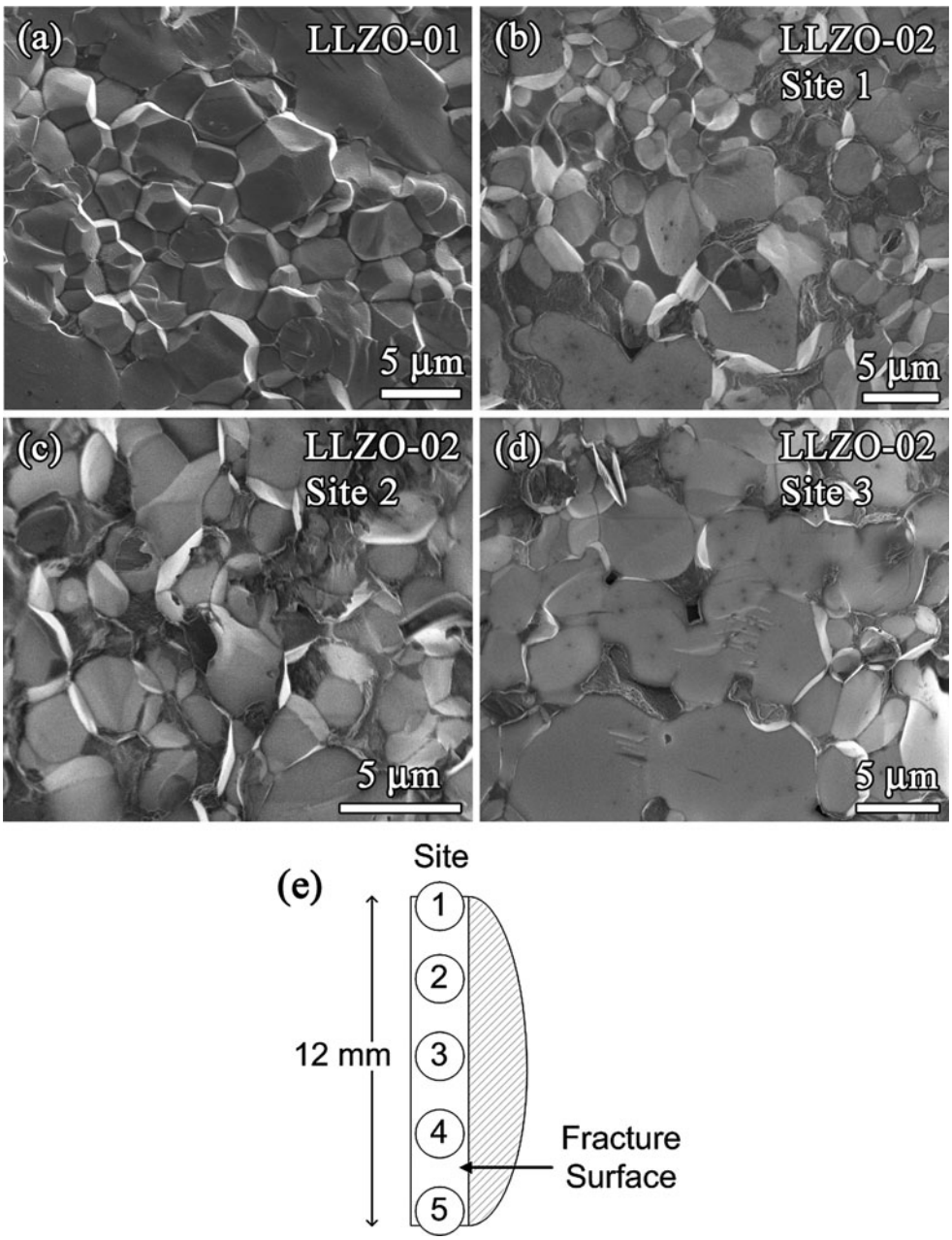

Fig. 1 The fracture surfaces for the hot-pressed specimens **a** LLZO-01 and **c–d** LLZO-02. The fracture surface of LLZO-02 was examined at **e** five different sites along the diametral fracture. Each site was roughly 3 mm apart and *sites 1* and *5* were approximately 0.5 mm from the specimen edge. For each micrograph the grain size was measured by the linear intercept method and a stereographic projection factor of 1.5 [33]

agreement with the general trend for bulk polycrystalline specimens [14, 19, 37–40].

Hardness measured via Vickers indentation testing

For indentation loads of 2.9 and 4.9 N, the average Vickers hardness (Eq. 1) of 10 indentations per load was 6.4 ± 0.4 and 6.2 ± 0.3 GPa for $P = 0.03$ and 5.2 ± 0.4 and 5.3 ± 0.4 GPa for $P = 0.06$, respectively. The hardness decreases with increasing porosity which is in agreement with the general trend for bulk polycrystalline specimens that H decreases with increasing volume fraction porosity, P [37, 40, 41].

Comparison of LLZO elastic moduli and hardness with literature data for other garnets

Since this is the first study of the elastic moduli and hardness for LLZO, it is important to compare values obtained in this study with the moduli and hardness of other garnets in the literature. For a given crystal structure the mechanical properties as a function of lattice parameter, a_0, can be represented by the empirical relationship

$$A = b_A a_0^{-m_A} \tag{2}$$

where mechanical property A is a function of Young's modulus, E bulk modulus, B shear modulus, G or hardness

Table 2 The density, volume fraction porosity, P, Young's modulus, E, bulk modulus, B, shear modulus, G, and Poisson's ratio, v, for the hot-pressed rectangular parallelepiped specimens included in this study as well as for polycrystalline garnet specimens from the literature

Specimen label	Density (g/cm^3)	P	Measurement technique	E (GPa)	B (GPa)	G (GPa)	v	Reference
LLZO-01a	4.97	0.03	RUS	149.8 ± 0.4	102.8 ± 0.3	59.6 ± 0.1	0.257 ± 0.002	This study
LLZO-02a	4.78	0.06	RUS	132.6 ± 0.2	97.7 ± 0.2	52.1 ± 0.04	0.274 ± 0.001	This study
$Y_3Fe_5O_{12}$ (YIG)	5.01	0.004	Sonic resonance technique	196.3	NA[a]	76.5	0.277	[16]
$Y_3Fe_5O_{12}$ (YIG)	4.572	0.115	Pulse-echo	157.7	117.4	61.8	0.276	[17]
$Y_{2.9}Fe_{5.1}O_{12}$	4.825	0.064	Pulse-echo	144.9	96.3	58.0	0.249	[17]
$Y_{2.7}Fe_{5.3}O_{12}$	4.901	0.043	Pulse-echo	98.4	71.3	38.8	0.270	[17]
$Y_{2.5}Fe_{5.5}O_{12}$	4.833	0.047	Pulse-echo	78.3	64.3	30.2	0.296	[17]

[a] Not available

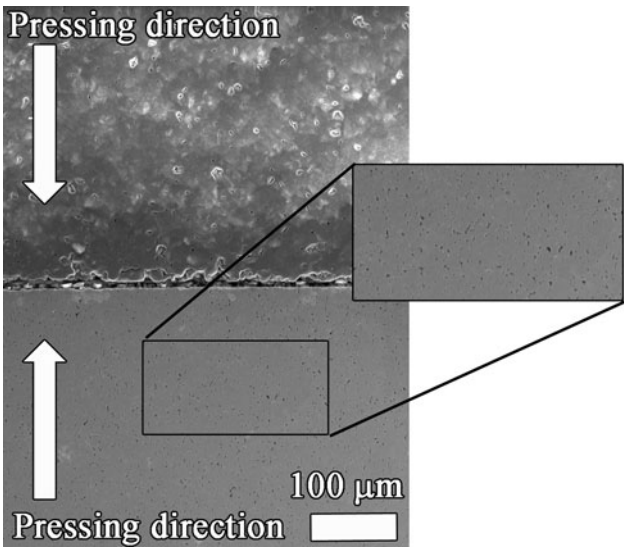

Fig. 2 Quasi-spherical porosity is evident on the polished cross section of the hot-pressed LLZO-01 specimen. The *arrows* indicate the hot pressing direction

H. Also b_A is a material-dependent constant and m_A is the exponent for the particular mechanical property [42–44]. For example, we use m_G to denote the exponent for the shear modulus, G, in Eq. (2).

The exponents m_B, m_G, and m_H (Eq. 2) depend on the crystal structure [42, 43, 45–48] (Table 3). The r^2 values for the literature data (Table 3) ranged from 0.983 to 0.999 for the moduli and hardness except for an r^2 of 0.886 for the FCC metals [45], thus Eq. (2) describes the decrease in B, G, and H with increasing a_0 relatively well. Although a direct relationship between Young's modulus and lattice parameter has not been illustrated in the open literature, a number of papers imply that in addition to the shear modulus, the Young's modulus is proportional to the interatomic distance [49–52]. The E and G values for garnets [36, 53–57], including data for LLZO, are plotted in Fig. 3a, b, respectively, as function of a_0. From both Fig. 3a, b, it is observed that the LLZO data are in excellent agreement with single crystal literature data for other garnets. The fit of Eq. (2) to the E and G data for all garnets shown including LLZO, yielded r^2 values of 0.936 and 0.914, respectively (Fig. 3a, b).

The relationship between elastic moduli and lattice parameter shown in this paper is empirical (Eq. 2); however, the elastic moduli are fundamentally related to atomic bonding. From the Born model for ionic bonding [13], the elastic moduli are second order partial derivatives of the binding energy [13], therefore the elastic moduli are proportional to the curvature of the binding energy curve. Since the binding energy can be written as a power law relationship of the separation distance, the elastic moduli can also be approximated with a power law relationship. This also implies that a larger separation distance between atoms, or a larger lattice parameter, will result in a lower Young's modulus.

In general, H decreases with increasing a_0 via a power law relationship (Eq. 2, Table 3). In particular, for the cubic garnet structure, the H versus a_0 relationship also follows Eq. (2) (Fig. 3c), as does the cubic garnet LLZO in this study. The hardness data for LLZO (this study) agrees relatively well with the single crystal literature data (Fig. 3c) [47]. However, the r^2 value of 0.840 indicates greater scatter in the H versus a_0 data fit to Eq. (2) (Fig. 3c) compared to the scatter observed in E (Fig. 3a) and G (Fig. 3b). For both single crystal and polycrystalline garnets, the observed scatter in H (Fig. 3c) may reflect the H dependence on the load, loading rate, the dislocation density, or residual stresses [58]. In general, for polycrystalline materials, H is also a function of grain size [59] and porosity [40].

The Poisson's ratio, v, (which unlike E, B, and G is relatively insensitive to P [60]) ranged from 0.226 to 0.295 for 21 single crystal and polycrystalline cubic garnets in the literature [36–38, 53–57, 61, 62]. For LLZO, in this study, the Poisson's ratio is bracketed by the v values for cubic garnets in the literature (Table 2).

Table 3 The exponents m_B, m_G, and m_H obtained by a least-squares fit to Eq. (2) for bulk modulus, B, shear modulus, G, and hardness, H data, respectively, from the literature for various cubic crystalline structures

Crystal structure	m_B^a (r^2, N)	m_G^b (r^2, N)	m_H (r^2, N)	Reference
Alkaline halide (rock salt)	NA[e]	3.2 ± 0.2 (0.983, 7)	3.0[d] (0.996[d], 11)	[22–25]
Alkaline earth oxides (rock salt)	3.3 ± 0.1 (0.998, 8)	NA[e]	3.0[d] (0.998[d], 4)	[22, 23]
Alkaline earth sulfides (rock salt)	NA[e]	NA[e]	3.0[d] (0.990, 4)	[28]
Face-center-cubic metals	NA[e]	6.4 ± 1.3[c] (0.886, 7)	NA[e]	[25]
Zincblende semiconductors	NA[e]	4.7 ± 0.1 (0.999, 9)	NA[e]	[25]

The coefficient of determination, r^2, along with the number of particular compositions of a given crystal structure included in the least-squares fit, N, are listed within the parentheses given to the right of each of the numerical values of the fitted exponents

[a] Gilman reported $m_B = 4$ for alkaline earth oxides [22]. Gilman did not report the r^2 values [22]

[b] Gilman reported $m_G = 4$ and 5 for alkaline halides and zinc blende semiconductors, respectively [22, 25]. Gilman did not report the r^2 values [22, 25]

[c] Exponent m_G value excluding thorium. If thorium is included in the analysis, then $r^2 = 0.758$ and $m_G = 5.2$. Gilman reported $m_G = 6.35$ when the plot included Th [25]

[d] Reported by Gilman [23]. All other exponents and r^2 values in this table were calculated by the present authors

[e] Not available

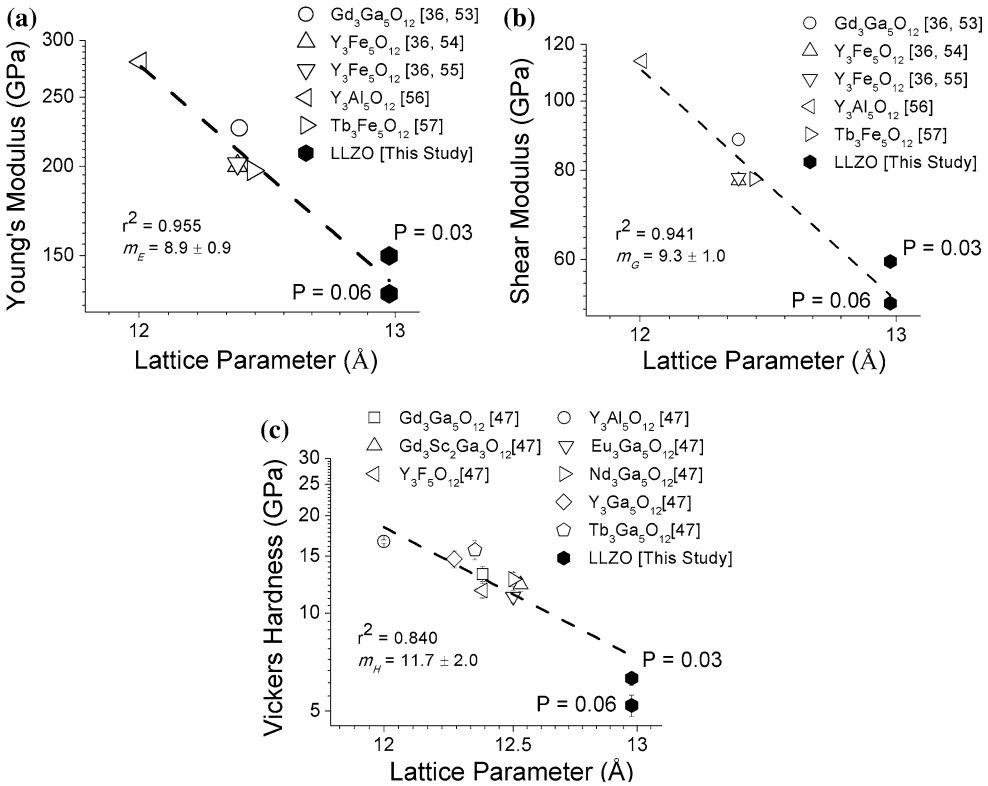

Fig. 3 The **a** Young's modulus, **b** shear modulus, and **c** hardness as a function of lattice parameter for the aggregate average values for single crystal garnet data in the literature (*open symbols*) and the LLZO garnet specimens in this study (*filled symbol*). In **a**, **b**, and **c**, the *dashed line* represents the least-squares fit of Eq. (2) to the data in this study and single crystal garnet in the literature [36, 47, 53–57]. The scatter in hardness, H, is likely due to the different mechanisms that can affect H ("Comparison of LLZO elastic moduli and hardness with literature data for other garnets" section)

Summary and conclusions

This work presents the first room temperature Young's modulus, shear modulus, bulk modulus, Poisson's ratio, and hardness values for $Li_7La_3Zr_2O_{12}$ garnet fabricated by hot pressing. Dense ($P = 0.03$–0.06) billets with mean grain sizes of roughly 5 μ were produced by hot pressing. For loads 2.9 and 4.9 N, the mean Vickers hardness, H, was 6.3 ± 0.3 and 5.2 ± 0.4 GPa for the $P = 0.03$ and 0.06 hot-pressed LLZO specimens, respectively. The Young's modulus was 149.8 ± 0.4 GPa for $P = 0.03$ (Table 2) and 132.6 ± 0.2 GPa for $P = 0.06$.

The values of E, B, G, and H for $Li_7La_3Zr_2O_{12}$ found in this study are consistent with the trend (Eq. 2) of a power law decrease in mechanical properties with increasing lattice parameter observed for other garnet materials in the

literature for E (Fig. 3a) [36, 53–57], B [36, 53–57], G (Fig. 3b) [36, 53–57], and H (Fig. 3c) [47].

The solid electrolyte $Li_7La_3Zr_2O_{12}$ (LLZO) has the potential to enable significant improvements in electrochemical energy technology. While much of the current literature on LLZO focuses on its electrical properties, we believe that a better understanding of the mechanical properties can accelerate the maturation of $Li_7La_3Zr_2O_{12}$ electrolyte membrane technology. For example, the mechanical properties must be well characterized and understood to enable the fabrication of relatively thin (10–100 μ) electrolyte membranes [63]. Also, the elastic modulus and hardness characterization of $Li_7La_3Zr_2O_{12}$ in this work enables the characterization of other important mechanical properties, such as the fracture toughness, which is currently underway in our group.

Acknowledgements We would like to acknowledge the financial support of the U.S. Army Research Office (ARO) and the Army Research Laboratory (ARL) under grant W911NF-10-2-0089-P00001.

References

1. Goodenough JB, Kim Y (2011) J Power Sources 196:6688
2. Kowalczk I, Read J, Salomon M (2007) Pure Appl Chem 79:851
3. Visco SJ, Katz BD, Nimon YS, De Jonghe LC (2007) US Patent 7,282,295 B2
4. Wolfenstine J, Allen JL, Sumner J, Sakamoto J (2009) Solid State Ion 180:961
5. Reddy JN (2006) An introduction to the finite element method, 3rd edn. McGraw-Hill Higher Education, New York
6. Shimonishi Y, Toda A, Zhang T, Hirano A, Imanishi N, Yamamoto O, Takeda Y (2011) Solid State Ion 183:48
7. Kotobuki M, Munakata H, Kanamura K, Sato Y, Yoshida T (2010) J Electrochem Soc 157:A1076
8. Kokal I, Somer M, Notten PHL, Hintzen HT (2011) Solid State Ion 185:42
9. Geiger CA, Alekseev E, Lazic B, Fisch M, Armbruster T, Langner R, Fechtelkord M, Kim N, Pettke T, Weppner W (2011) Inorganic Chem 50:1089
10. Murugan R, Thangadurai V, Weppner W (2007) Angew Chem Int Ed 46:7778
11. Rangasamy E, Wolfenstine J, Sakamoto JS (2011) Solid State Ion 206:28
12. Rietveld HM (1969) J Appl Crystallogr 2:65
13. Wachtman JB, Cannon WR, Matthewson MJ (2009) Mechanical properties of ceramics, 2nd edn. Wiley, Hoboken
14. Ren F, Case ED, Morrison A, Tafesse M, Baumann MJ (2009) Philos Mag 89:1163
15. Ni JE, Case ED, Khabir KN, Stewart RC, Wu C-I, Hogan TP, Timm EJ, Girard SN, Kanatzidis MG (2010) Mater Sci Eng B 170:58
16. Ren F, Case ED, Sootsman JR, Kanatzidis MG, Kong H, Uher C, Lara-Curzio E, Trejo RM (2008) Acta Mater 56:5954
17. Ren F, Case ED, Ni JE, Timm EJ, Lara-Curzio E, Trejo RM, Lin C-H, Kanatzidis MG (2009) Philos Mag 89(2):143
18. Vdovychenko OV, Voropaev VS, Slipenyuk AN (2006) J Mater Sci 41:8329. doi:10.1007/s10853-006-1019-2
19. Ni JE, Ren F, Case ED, Timm EJ (2009) Mater Chem Phys 118:459
20. Davulis PM, Shyam A, Lara-Curzio E, Pereira da Cunha M (2008) IEEE Int Ultrason Symp Proc 1–4:2150
21. Drymiotis FR (2010) Int J Mod Phys B 24:1047
22. Lein HL, Andersen ØS, Vullum PE, Lara-Curzio E, Holmestad R, Einarsrud M-A, Grande T (2006) J Solid State Electrochem 10:635
23. Pestka KA, Scott ES, Le Page Y (2011) AIP Adv 1:032154
24. Pestka KA, Maynard JD, Soukiassian A, Xi XX, Schlom DG, Le Page Y, Bernhagen M, Reiche P, Uecker R (2008) Appl Phys Lett 92:111915
25. Pham HH, Williams ME, Mahaffey P, Radovic M, Arroyave R, Cagin T (2011) Phys Rev B 84:064101
26. Radovic M, Lara-Curzio E (2004) J Am Ceram Soc 87:2242
27. Radovic M, Barsoum MW, Ganguly A, Zhen T, Finkel P, Kalidindi SR, Lara-Curzio E (2006) Acta Mater 54:2757
28. Salvador JR, Yang J, Shi X, Wang H, Wereszczak AA, Kong H, Uher C (2009) Philos Mag 89:1517
29. Flynn K, Radovic M (2011) J Mater Sci 46:2548. doi:10.1007/s10853-010-5107-y
30. Gudlur P, Forness A, Lentz J, Radovic M, Muliana A (2012) Mater Sci Eng A 531:18
31. Barsoum MW, Radovic M, Zhen T, Finkel P, Kalidindi SR (2005) Phys Rev Lett 94:085501
32. McClellan KJ, Chu F, Roper JM, Shindo I (2001) J Mater Sci 36:3403. doi:10.1023/A:1017947625784
33. Fullman RL (1953) Trans AIME 197:447
34. Houston B, Strakna RE, Belson HS (1968) J Appl Phys 39:3913
35. Einspruch NG, Manning RJ (1963) J Acoust Soc Am 35:215
36. Simmons G, Wang H (1971) Single crystal elastic constants and calculated aggregate properties: a handbook. The MIT Press, Cambridge
37. Chou HM, Case ED (1988) J Mater Sci Lett 7:1217
38. Sharma PU, Modi KB (2010) Phys Scr 81:015601
39. Dey A, Mukhopadhyay AK (2011) Int J Appl Ceram Technol 8:572
40. Rice RW (1998) Porosity of ceramics. Marcel Dekker Inc., New York
41. Hoepfner TP, Case ED (2003) Ceram Int 29:699
42. Gilman JJ (1969) Micromechanics of flow in solids. McGraw Hill, New York
43. Gilman JJ (2009) Chemistry and physics of mechanical hardness. Wiley, Hoboken
44. Wooster WA (1953) Rep Prog Phys 16:62
45. Gilman JJ (1963) Natl Bureau Stand Monogr 59: 79
46. Ruffa AR (1963) Phys Rev 130:1412
47. Sirdeshmukh DB, Subhadra KG, Rag KK, Rao TT (1995) Cryst Res Technol 30:861
48. Winkler HGF (1955) Struktur und Eigenshaften der Kristalle. Springer Vaerlag, Berlin
49. Liu M, Shi B, Guo J, Cai X, Song H (2003) Scr Mater 49:167
50. Vijh AK (1975) J Mater Sci 10:1087. doi:10.1007/BF00823227
51. Ravinder D, Vijaya Kumar K, Boyanov BS (1999) Mater Lett 38:22
52. Makishima A, Mackenzie JD (1973) J Non-Cryst Solids 12:35
53. Graham LJ, Change R (1970) J Appl Phys 41:2247
54. Bateman TB (1966) J Appl Phys 37:2194
55. Clark AE, Strakna RE (1961) J Appl Phys 32:1172
56. Mezeix L, Green DJ (2006) Int J Appl Ceram Technol 3:166
57. Saunders GA, Parker SC, Benbattouche N, Alberts HI (1992) Phys Rev B 46:8756
58. Gilman JJ (1973) In: Westbrook JH, Conrad H (eds) The science of hardness testing and it's research applications. American Society for Metals, Metals Park, p 51

59. Rice RW (2000) Mechanical properties of ceramics and composites. Marcel Dekker Inc., New York
60. Boccaccini AR (1994) J Am Ceram Soc 77:2779
61. Verma RK (1960) J Geophys Res 65:757
62. Soga N (1967) J Geophys Res 72:4227
63. Birke P, Salam F, Doring S, Weppner W (1998) Solid State Ion 91:149